Astron. Astrophys. 171, 49–65 (1987)

ASTRONOMY AND ASTROPHYSICS

A gravitational lens origin for AGN-variability? Consequences of micro-lensing ⋆

P. Schneider [1,2,⋆⋆] **and A. Weiss** [1]

[1] Max-Planck-Institut für Physik und Astrophysik, Institut für Astrophysik, Karl-Schwarzschild-Strasse 1, D-8046 Garching bei München, Federal Republic of Germany
[2] Joint Institute for Laboratory Astrophysics, University of Colorado, Boulder, CO 80309, USA

Received May 28, accepted July 11, 1986

Summary. The gravitational action of an ensemble of stars (e.g., in a galaxy) on the light of a compact background source is studied, in extension of previous studies by Paczyński (1986) and Kayser et al. (1986). We compute representative light curves of sources which move relative to the star field, amplification probabilities and the distribution of the amplification factor as a function of the relative source position. Our numerical scheme enables us to consider very large optical depth or, equivalently, a large number ($\lesssim$10 000) of stars. Whereas for moderate optical depth a typical light-curve is characterized by rather quiet behaviour most of the time, interrupted by sudden "outbursts", sources behind dense star fields tend to show a very irregular flickering, without very dramatic changes of their apparent luminosity. The amplification probability function shows a much more complex behaviour than the analytically estimated I^{-2} dependence. We find a rather pronounced tendency of clustering of caustics in the source plane.

In the light of recent results which indicate that a large fraction of quasars is gravitationally micro-lensed, we propose the time-dependent amplification by micro-lenses to be a reasonable explanation for variability in at least some active galactic nuclei; in particular, our results support the recent hypothesis (Ostriker and Vietri, 1985) that the BL-Lac objects may be due to selective amplification of quasars.

Key words: quasars – galaxies – gravitational lenses – active galaxies – gravitation

1. Introduction

Since the discovery of the first gravitational lens (Walsh et al., 1979) it was realized that individual stars in the lensing galaxy can significantly influence the properties of the images of the lensed source (Chang and Refsdal, 1979, 1984). Besides causing difficulties in interpreting observed lens cases, this micro-lensing could be an important tool to investigate the matter contents of galaxies (Gott, 1981; Canizares, 1981; Young, 1981). In addition, compact objects – e.g. in galaxies – are efficient amplifiers of background compact sources (Canizares, 1981, 1982; Vietri and Ostriker, 1983; Vietri, 1985; Schneider, 1986a–c) and can therefore have a significant impact on source counts.

Most investigations of micro-lensing were done by considering only one compact object acting on light rays; however, this is reasonable only if the "optical depth" to micro-lensing κ (defined below in Sect. 2) is very small. The optical depth at the image positions of multiple imaging lenses is expected not to be small; hence, one is mostly interested in cases of large κ. Investigations of these situations necessarily require time consuming numerical simulations. Young (1981) applied Monte-Carlo methods to this lensing problem; he considered the shape of the image of an extended source viewed through a star field in a galaxy. However, this method allows to treat only a limited number of cases and is not useful for statistical investigations of the amplification factor of the images.

In quite a different manner Paczyński (1986) tried to find (numerically) all images of a source behind a random field of stars by solving the lens equation. Although this method gives information on the position and amplification factors of individual images, it is subject to several restrictions. First, it is only applicable to point sources. Secondly, it is not known a priori how many solutions of the lens equation exist, and his method cannot assure to find all the brightest images. If one considers a star field of N_* stars, the number of solutions of the lens equation is approximately N_*. Moreover, the computations have to be done for every particular relative position of the source and is, therefore, very time consuming and not well suited for statistical considerations. He obtained light curves of point sources which change their position relative to the lens which are the most probable observable in micro-lensing situations.

Kayser et al. (1986, hereafter KRS) reconsidered the problem tackled by Paczyński by using the ray shooting method (Schneider and Weiss, 1986). This method allows to consider extended sources, one can estimate the error introduced by considering only a limited number of micro-images and the total amplification factor is obtained for a whole range of source positions simultaneously. The fact that no information about the position of the micro-images is obtained with this method is unimportant, since in typical lensing situations one can never resolve them observationally. KRS obtained light curves for several source sizes

Send offprint requests to: A. Weiss

⋆ Dedicated to R. Kippenhahn and H.U. Schmidt on the occasion of their joint 120th birthday

⋆⋆ Present address

as well as important information about the lensing geometry, e.g. the critical lines (caustics) in the source and lens planes.

By improving the numerical method, we have extended the work of KRS which is limited to moderate optical depth $\kappa \leqq 0.4$. We obtain detailed information about the total amplification factor of a macro-image (i.e. the sum of all micro-images) as a function of the source position, the amplification probability function and typical light curves for several source sizes. Our computational scheme allows to treat rather high optical depth or, equivalently, a large number of objects in the star field, and to determine the amplification of extended sources with very high accuracy.

In Sect. 2 we briefly describe the model and give the relevant equations. The numerical method is outlined in Sect. 3. We estimate the error caused by considering a finite number of stars and show that it is completely negligible for our calculations (Sect. 4). Results are given in Sect. 5, where we display the amplification factor as a function of source position, from which typical light curves and amplification probabilities are obtained. We conclude with a discussion of the applicability of our results to explain the variability of at least some compact active galactic nuclei.

2. Description of the model

Gravitational lensing by a galaxy which is composed of compact objects [i.e. objects of size $< \xi_0$, see Eq. (1)] and interstellar matter is a two scale problem: the gravitational field of the galaxy as a whole produces one or several macro-images of a background source, the relevant length scale being 1 –10 kpc. The light bundle corresponding to a macro-image is subject to the gravitational deflection of individual stars which cause a splitting into a large number of micro-images. Here, the relevant length scale is

$$\xi_0 = \left(\frac{4GM}{c^2}\frac{D_d D_{ds}}{D_s}\right)^{1/2} \tag{1}$$

(Refsdal, 1964), where M is the typical mass of the compact objects and D_d, D_s, and D_{ds} are, respectively, the angular diameter distance to the lens and source, and from the lens to the source. For solar mass objects, one typically obtains $\xi_0 \sim 10^{16}$ cm for cosmological distances of sources and lens. It is therefore reasonable in considerations of micro-lensing to treat the large scale gravitational field of the galaxy in linear approximation while the deflection of a number of stars around the macro-image position is explicitely computed. Since the deflection angle of a compact object ("Einstein angle") is a diverging function of the impact parameter of a light ray, there are, in principle, about as many micro-images as there are stars in the galaxy. However, they are of quite different relative flux, which decreases with the distance r_* of a star from the macro-image position as r_*^{-4}. Due to this rapid decline of the amplification of images, it is sufficient to consider only a limited number of stars and micro-images; the error introduced by this is estimated in Sect. 4 below.

In the following we assume that all stars in the galaxy are of equal mass M; the galaxy can then be described by just two functions, the surface mass density κ_c of the interstellar matter and that of the compact objects κ_*, both measured in units of the critical surface mass density

$$\Sigma_0 = \left(\frac{4\pi G}{c^2}\frac{D_d D_{ds}}{D_s}\right)^{-1} \tag{2}$$

(cf. Young, 1981, KRS). Measuring all lengths in the lens plane in units of ξ_0 (1) and all lengths in the source plane in units of

$$\chi_0 = \xi_0 D_s / D_d , \tag{3}$$

the dimensionless number density of stars n_* (number of stars per dimensionless area) is related to κ_* by $\pi n_* = \kappa_*$.

Let $\kappa_s = \kappa_c + \kappa_*$ be the surface mass density of the smoothed-out galaxy; macro-images are then described by the lens equation

$$\boldsymbol{x} = \boldsymbol{r} - \boldsymbol{\alpha}_s(\boldsymbol{r}) , \tag{4}$$

where the "smooth" deflection $\boldsymbol{\alpha}_s(\boldsymbol{r})$ is related to κ_s through

$$\boldsymbol{\alpha}_s(\boldsymbol{r}) = \pi^{-1} \nabla \int_{\mathbb{R}^2} d^2 r' \kappa_s(\boldsymbol{r}') \ln|\boldsymbol{r} - \boldsymbol{r}'| \tag{5}$$

(cf. Schneider, 1985; Blandford et al., 1986); $\boldsymbol{x}$ is the dimensionless source position vector and $\boldsymbol{r}$ the impact vector in the lens. A solution of (4) for given source position $\boldsymbol{x}$ is called macro-image. Consider now a macro-image $\boldsymbol{r}_I$ for $\boldsymbol{x} = \boldsymbol{x}_I$. Defining $\boldsymbol{x}' = \boldsymbol{x} - \boldsymbol{x}_I$, $\boldsymbol{r}' = \boldsymbol{r} - \boldsymbol{r}_I$, the splitting into micro-images is described by

$$\boldsymbol{x}' = \begin{pmatrix} 1-\kappa_c-\gamma & 0 \\ 0 & 1-\kappa_c+\gamma \end{pmatrix} \boldsymbol{r}' - \sum_{i=1}^{N_*} \frac{\boldsymbol{r}' - \boldsymbol{r}_i'}{|\boldsymbol{r}' - \boldsymbol{r}_i'|^2} \tag{6}$$

(see KRS), where $\kappa_c = \kappa_c(\boldsymbol{r}_I)$ is the local density of the interstellar matter, γ is the shear produced by the galaxy as whole and is given in terms of $\boldsymbol{\alpha}_s(\boldsymbol{r}_I)$ by

$$\gamma^2 = \frac{1}{2}\left[\left(\frac{\partial \alpha_{s,1}}{\partial r_1}\right)^2 + 2\left(\frac{\partial \alpha_{s,1}}{\partial r_2}\right)^2 + \left(\frac{\partial \alpha_{s,2}}{\partial r_2}\right)^2\right] , \tag{7}$$

and the $\boldsymbol{r}_i'$ are the position vectors relative to $\boldsymbol{r}_I$ of the N_* stars explicitely taken into account.

Equation (6) can now be used, applying the ray-shooting method described below (Sect. 3), to obtain light curves and amplification probabilities of extended sources. Beside of the source size b, these quantities depend on the local density of interstellar matter κ_c, the galactic shear γ and the number density of stars n_*. As was shown by Paczyński (1986) there is a scaling procedure which allows the determination of the physical quantities (light curves, amplification probability) for a one-parameter class of models $(b, \kappa_c, \gamma, n_*)$ simultaneously. That such a relation should exist is clear from the fact that a homogeneous sheet of matter simply acts as an ideal lens, thus changing merely the length scales of the problem under consideration. In Appendix A it is shown that two models with different κ_c, κ_c, and κ_c', say, are equivalent, if the following relations for the shears, star densities and source sizes are satisfied,

$$\gamma' = \left(\frac{1-\kappa_c'}{1-\kappa_c}\right)\gamma , \tag{7a}$$

$$n_*' = \left|\frac{1-\kappa_c'}{1-\kappa_c}\right| n_* , \tag{7b}$$

$$b' = \left|\frac{1-\kappa_c'}{1-\kappa_c}\right|^{1/2} b . \tag{7c}$$

The amplification factors are related through

$$I' = \left(\frac{1-\kappa_c'}{1-\kappa_c}\right)^2 I \tag{7d}$$

(for details see Appendix A). These scaling relations allow to generalize the results shown in Sect. 5 for a whole class of models.

3. The numerical method

As already mentioned, we computed the amplification factor of extended sources as a function of source position by using the ray-shooting method, which was described by Schneider and Weiss (1986), Schneider (1986b), and KRS. With this method, a regular grid of points $\boldsymbol{r}$ (in the following we drop the primes on $\boldsymbol{r}$ and $\boldsymbol{x}$) of the lens plane is mapped via (6) onto the source plane. These "light rays" are then "collected" in pixels in the source plane, and the number of rays in one pixel is then, up to an overall scaling factor, the total amplification factor of a source of uniform brightness whose (dimensionless) area equals the size of a pixel, provided the area which the grid-points cover in the lens plane is as large as to cover all possible images of the source at the position of the pixel. In the situation we consider here, this last condition is not strictly satisfied, due to the divergence of the Einstein angle; hence, there are very distant micro-images not covered by the grid. In the next Section it is shown that in our calculation this "diffuse flux" is always very small.

We considered a square-shaped area of length L_s in the source plane and divided it into N_p^2 pixel, where as a rule $N_p = 512$, except in one test case where $N_p = 1024$. The corresponding "sources" are thus squares of length $b = L_s/N_p$. If the deflecting mass distribution were smoothed out, a rectangle of sides L_x^0 and L_y^0 would be mapped onto the square in the source plane, where $L_x^0 = L_s|1-(\kappa_c+\kappa_*+\gamma)|^{-1}$ and $L_y^0 = L_s|1-(\kappa_c+\kappa_*-\gamma)|^{-1}$. But due to the grainyness of the deflector, a much larger area of the lens plane must be mapped onto the source plane.

We proceeded as follows. In an ellipse with semi-axis B and D we randomly distributed $N_* = BD\kappa_*$ stars, where the axial ratio was taken to be $B/D = q$, where

$$q = \left|\frac{1-(\kappa_c+\kappa_*-\gamma)}{1-(\kappa_c+\kappa_*+\gamma)}\right|, \tag{8}$$

such that it would be mapped onto a circle if the smoothed-out matter acts as deflector. Within this ellipse, a rectangle of sides L_x and L_y was chosen, where $L_x, L_y \gg L_x^0, L_y^0$, and $L_x/L_y = q$. On this "shooting area", a grid of $N_1\ N_2$ points (i.e., light rays) was mapped onto the source plane ($N_1/N_2 = q$), and the number of rays which hit each pixel was counted. The amplification of a source corresponding to a pixel in which $N_{\rm ray}$ rays are counted is $I = f_{\rm sc} N_{\rm ray}$, where $f_{\rm sc} = L_x L_y/(N_1 N_2 b^2)$.

If the mapping of the grid points is made straightforwardly using (6), one very soon runs into severe numerical limitations. Since one would like to have $f_{\rm sc}$ rather small to get rid of significant statistical errors in $N_{\rm ray}$ (note that, since a regular grid is mapped, the statistical uncertainties are much smaller than those from Poisson statistics, $N_{\rm ray}^{1/2}$, see KRS), a large number of grid points are taken (on the order of 10^9 to 10^{11}). Since one also wants to consider large optical depths $\kappa = \kappa_*|1-\kappa_c|^{-1}$, N_* can also be large (we took up to 8000 stars). Hence, in some of our models, up to $\sim 10^{14}$ single star deflection angles have to be computed according to (6), which is far beyond reasonable computing facilities.

A way out of those difficulties is provided by the following method: We divided the shooting area in a number $n_1 \cdot n_2$ of shooting squares of length $a = L_x/n_1 = L_y/n_2$. The deflection angle of the stars [i.e., the sum in (6)] was then split into two parts: the deflection caused by stars within a square of length $\sim 15a$ centered on the corresponding shooting square and the deflection of all other (distant) stars. While the first part was computed directly adding the individual deflection angles of the "near" stars, the second contribution for each grid point within the shooting square was estimated by expanding the deflection of all distant stars about the center of the shooting square up to second order. We have checked that this expansion method introduces no noticeable error in the final results; at this point we like to point out that the color graphics used to display our results (Sect. 5) also provides an excellent error diagnostics.

Since we probed a large area of the lens plane, there are a lot of shooting squares which contain no grid point which hits the collection area in the source plane. Therefore, for each shooting square we first mapped 9 grid points and tested whether at least one of them is imaged within or near the collection area. If this was the case, all grid-points of the shooting square had been mapped. With this pre-selection method, it was possible to enlarge the shooting area of the lens plane considerably.

4. Estimation of the neglected diffuse flux

A star well away from that light beam which would be produced by the smoothed out matter distribution $\kappa_s(\boldsymbol{r})$ causes a (faint) micro-image of the source. We have estimated the flux of all these micro-images which are produced by stars outside of the ellipse B, D.

Consider a star at $\boldsymbol{r}_*$ outside the ellipse. The mapping near that star can be obtained approximately by treating all other stars as being smoothed out; the lens equation then reads

$$\boldsymbol{x} \approx \begin{pmatrix} 1-\kappa_s-\gamma & 0 \\ 0 & 1-\kappa_s+\gamma \end{pmatrix} \boldsymbol{r} - \frac{\boldsymbol{r}-\boldsymbol{r}_*}{|\boldsymbol{r}-\boldsymbol{r}_*|^2}. \tag{9}$$

Since $\boldsymbol{r}_*$ lies outside the ellipse, one has $|\Delta\boldsymbol{r}| = |\boldsymbol{r}-\boldsymbol{r}_*| \ll \boldsymbol{r}_*$, and therefore,

$$\boldsymbol{x} \approx \boldsymbol{R}_* - \frac{\Delta\boldsymbol{r}}{|\Delta\boldsymbol{r}|^2}, \tag{10}$$

where

$$\boldsymbol{R}_* = \begin{pmatrix} 1-\kappa_s-\gamma & 0 \\ 0 & 1-\kappa_s+\gamma \end{pmatrix} \boldsymbol{r}_*. \tag{11}$$

Consider the source at $\boldsymbol{x} = 0$; one then obtains

$$\Delta\boldsymbol{r} = \boldsymbol{R}_*/|\boldsymbol{R}_*|^2.$$

From the definition of the amplification factor, $I = |\det(\partial\boldsymbol{x}/\partial\boldsymbol{r})|^{-1}$ one finds $I = |\Delta\boldsymbol{r}|^4 = |\boldsymbol{R}_*|^{-4}$ (see Schneider, 1986c). The diffuse flux f_d is then obtained by summing up the amplification factors of all micro-images produced by stars outside the ellipse with semi-axis B and $D = B/q$. Hence,

$$f_d = n_* \int d^2r\, |\boldsymbol{R}_*(\boldsymbol{r})|^{-4}, \tag{12}$$

where the integral extends over $\mathbb{R}^2$ minus the ellipse. Introducing a new coordinate frame (ϱ, ϕ) by $(r_1, r_2) = \varrho\,(B\cos\phi, D\sin\phi)$, one finds for $|\boldsymbol{R}_*|$

$$|\boldsymbol{R}_*|^2 = \varrho^2 \tilde{B}^2 (1-\kappa_s-\gamma)^2, \tag{13}$$

where (8) was used. Thus, the integral (12) can be written as

$$f_d = n_* 2\pi \tilde{B}\tilde{D} \int_1^\infty \varrho\, d\varrho\, \tilde{B}^{-4} \varrho^{-4} (1-\kappa_s-\gamma)^{-4}, \tag{14}$$

which is easily evaluated. Using (8) again, one finally obtains

$$f_d = \kappa_* (\tilde{B}\cdot\tilde{D})^{-1} \langle I_s\rangle^2, \tag{15}$$

where

$$\langle I_s\rangle = |(1-\kappa_s)^2 - \gamma^2|^{-1} \tag{16}$$

Table 1. Description of the models shown in Figs. 1–3. See text for details

Model	a	b	c	d	e	f	g	h	i	j	k	l
κ_*	0.2	0.2	0.5	0.5	0.7	0.8	0.2	0.2	0.2	0.8	1.5	1.3
κ_c	0.0	0.0	0.0	0.0	0.0	0.0	0.5	0.3	0.2	2.0	0.0	0.0
γ	0.0	0.0	0.0	0.0	0.0	0.0	0.0	0.3	0.4	0.0	0.0	0.0
b	0.025	0.025	0.0125	0.0125	0.0125	0.0125	0.0125	0.0125	0.0125	0.0375	0.0125	0.0125
N_*	245	245	288	288	2520	8000	500	300	400	320	5400	4680
ε [%]	0.08	0.08	1.04	1.04	0.65	0.60	0.27	0.25	0.15	0.19	0.50	1.20
$\langle I_S \rangle$	1.56	1.56	4.00	4.00	11.1	25.0	11.1	6.25	5.00	0.31	4.00	11.1
$\langle I \rangle$	1.51	1.68	3.11	3.81	15.1	17.4	11.7	3.71	3.76	0.31	2.65	10.5
f_{sc}^{-1}	791.1	791.1	791.1	791.1	351.6	351.6	156.3	459.2	208.0	316.4	258.3	258.3
Δm_{min}	0.0	0.0	0.0	0.0	1.0	1.4	1.4	0.6	0.6	− 4.0	− 0.2	1.0
Δm_{max}	3.0	3.0	3.0	3.0	4.0	4.4	4.4	3.6	3.6	2.0	3.3	4.0
L_S	12.8	12.8	6.4	6.4	6.4	6.4	6.4	6.4	6.4	19.2	6.4	6.4

is the amplification factor of the source for the smooth mass distribution, and should also be the average amplification in our models. Note that the final result (15) agrees with Eq. (41) of Katz et al. (1986), who derived that with a completely different method.

The parameters $\tilde{B}$ and $\tilde{D}$ of the ellipse used in the above computations should not be confused with the ellipse (B, D) in which the N_* were distributed, since $(\tilde{B}, \tilde{D})$ strictly should agree with the shooting area. However, since the shooting area was chosen to be a rectangle, (15) only gives an estimate of the diffuse flux (although a rather good one!). Choosing $\pi \tilde{B}\tilde{D} \sim L_x L_y$, we roughly set $\tilde{B}\tilde{D} \sim BD/3$. Let $\varepsilon = f_d/\langle I_s \rangle$ be the *relative* diffuse flux, one can estimate the number of stars N_* necessary to get the relative diffuse flux below ε:

$$N_* = \kappa_* BD \approx 3\varepsilon^{-1} \kappa_*^2 \langle I_s \rangle . \tag{17}$$

This shows that N_* can be quite large. E.g., if one takes $\varepsilon = 0.01$, one obtains for a model with $\kappa_c = \gamma = 0$

$$N_* = 300 \left(\frac{\kappa_*}{1 - \kappa_*} \right)^2 ,$$

which is 4800 for $\kappa_* = 0.8$. As seen from Table 1, we took for this model $N_* = 8000$; hence, the diffuse flux we neglected is well below 1 %.

5. Results

Applying the method described in Sect. 3, we have computed the amplification factor as a function of the source position for several values of the parameters κ_*, κ_c and γ. The parameters of the 12 models we present here are listed in Table 1, and various results of the calculations are given in Tables 1 and 2, and Figs. 1–3, and will be discussed below. As is seen from Table 1, we have considered optical depths up to 0.8; even in this case, the relative diffuse flux ε was very low, 0.6 %. In most cases, the smallest source size we considered, b, was taken to be 0.0125, but in some cases, b was chosen larger in order to have more stars in the rectangle of size L_x^0, L_y^0 (cf. Sect. 3). The quantity f_{sc}^{-1} is the number of rays per pixel which correspond to an amplification of unity. In all cases considered here, one has $\langle I_s \rangle f_{sc}^{-1} > 1000$, which corresponds to a Poisson statistics error of ~ 3 %; however, since for our method the error is much less than Poissonian (cf. KRS), we except it to be well below the 1 % error level.

5.1. *Amplification as a function of source position*

In Fig. 1 a–l, we have plotted the amplification factor as a function of the source position. For this, the magnification

$$\Delta m = 2.5 \lg I \tag{18}$$

was coded as a colour: the interval between Δm_{min} and Δm_{max} (see Table 1) was divided into 5 equal parts, corresponding to (increasingly) blue, grayish blue, green, yellow, and red, and within these 5 intervals, the 10 shades of the colour increases with Δm regularily. (Example: In Fig. 1 h, $\Delta m_{min} = 0.6$, $\Delta m_{max} = 3.6$; therefore, the interval between $\Delta m = 1.8$ and $\Delta m = 2.4$ is shown as green, and each shade of green corresponds to an interval of $\Delta m = 0.06$.) Pixels with $\Delta m > \Delta m_{max}$ are shown in white, those with $\Delta m < \Delta m_{min}$ in black. The length of the regions L_s of the source plane shown are also listed in Table 1. (Note that, for convenience, we have defined Δm to be positive for enhanced source brightness, as opposed to the usual convention.)

Basically, the Figures speak for themselves, and one gets a very good idea of the physical situation just by studying them carefully. One can see a variety of critical structures (cf. Blandford et al., 1986); for low optical depth (e.g., Fig. 1 a and b), one obtains the characteristic Chang-Refsdal (1979, 1984) critical lines and those corresponding to double stars (Schneider and Weiss, 1986). Although there is no external (galactic) shear in Fig. 1 a and b, the Chang-Refsdal structures appear due to the shear caused by the neighbouring stars. As an example of critical lines caused by double stars, consider the critical region to the lower right of the center of Fig. 1 a. We have verified that this isolated structure, together with the two triangle-shaped regions in the relative upper right and lower left direction are caused by a double star with (in the notation of Schneider and Weiss, 1986) $\chi < 8^{-1/2}$. In particular, this explains the occurrence of small triangle-shaped critical structures in the Figures. For higher optical depth of micro-lenses, it is no longer possible to direct to a specific constellation of compact objects which accounts for a critical structure; the critical structures become more complex with increasing κ.

One of the most surprising results of the computations is visible in all cases: there is a strong tendency of critical structure to cluster. E.g., in Fig. 1 c and d there are very crowded regions, side by side with a surprisingly large area where no critical line is found. This behaviour is explained by the fact that the formation

Table 2. The factor $Q(24)$ for different source sizes and power law indices

α	Source size	a	b	c	d	e	f	g	h	i	j	k	l
2.5	b	1.46	1.53	2.16	2.42	4.28	4.63	4.20	2.24	2.32	1.24	2.00	3.65
	$10b$	1.39	1.46	2.06	2.32	4.23	4.60	4.01	2.14	2.19	1.01	1.87	3.59
	$100b$	1.31	1.33	1.78	1.89	4.44	4.71	3.83	2.01	1.92	0.65	1.45	3.73
3.0	b	2.69	2.82	5.48	6.80	19.4	22.8	20.7	6.00	6.38	2.10	4.65	14.2
	$10b$	2.22	2.39	4.76	6.05	18.6	22.1	17.8	5.00	5.30	1.23	4.00	13.6
	$100b$	1.71	1.81	3.48	4.25	19.1	22.1	14.8	4.08	4.02	0.46	2.54	13.6
3.3	b	4.50	4.54	10.3	13.4	49.4	61.3	58.5	12.1	12.8	3.15	8.30	33.2
	$10b$	3.17	3.40	8.23	11.3	46.2	58.2	45.6	8.71	9.45	1.45	6.63	30.8
	$100b$	2.02	2.26	5.32	7.15	46.5	56.6	33.7	6.31	6.35	0.38	3.65	29.8
3.6	b	8.42	7.92	20.6	27.7	128	168	174	26.7	27.7	4.97	15.6	79.0
	$10b$	4.81	5.04	14.6	21.6	116	155	120	15.6	17.4	1.73	11.4	70.7
	$100b$	2.41	2.82	8.25	12.3	114	147	77.8	9.81	10.2	0.32	5.34	65.9
4.0	b	22.5	18.7	56.2	77.0	467	663	801	86.5	85.7	9.83	38.8	258
	$10b$	9.15	9.02	32.8	53.0	404	586	454	36.6	41.5	2.26	24.7	219
	$100b$	3.06	3.82	15.1	26.3	383	529	241	17.8	19.4	0.26	9.11	192

of a critical line is due to the derivative of the deflection angle, whereas its position is determined by the deflection itself. The deflection, however, has the tendency to intensify any random density enhancement of compact objects in the lens plane onto the source plane, due to the mutual gravitational attraction.

This clustering has, at least, two severe consequences for our analysis. First, due to the large-scale patterns, the area of the source plane shown can not be expected to represent the *average* structure of the source plane, but it shows a *randomly* selected part of the amplification function. As a measure for the deviation of the considered area from the average behaviour, we have computed the mean amplification $\langle I\rangle$ over the area shown in each case and compared that in Table 1 to the average amplification $\langle I_s\rangle$ (16), which is the amplification of the macro-image, due to flux-conservation. As can be seen from Table 1, the deviation of $\langle I\rangle$ from $\langle I_s\rangle$ is in some cases considerable. For this reason, we have presented, for two sets of physical parameters, two computations each (i.e. case a and b, and c and d, respectively), which can be seen to be mutually different qualitatively; e.g., there is a much larger concentration of critical lines in case d than in case c.

A second consequence of this clustering is directly related to observation. Since there are large regions of the source plane where the amplification function is very flat a source moving relative to the lens (and, therefore, changing its position in the source plane) can have a much more flatter light curve than one would expect from simple independent point masses considerations. In addition, since the patterns of the critical lines are frequently much larger than, say, a Chang-Refsdal critical region, one can also obtain flat light curves at considerable amplification. This is shown below.

5.2. *Light curves*

In Fig. 2a–l we have plotted the magnification Δm of sources of size b, $10b$ and $50b$, as a function of the dimensionless distance along several straight lines through the source plane, where the unit of distance is χ_0 (3). However, if the effective transverse velocity is v [see KRS, Eq. (B9)], the curves shown in Fig. 2 are light curves $\Delta m(t)$, where the unit of time is

$$\tau_0 = \chi_0/v\,. \tag{19}$$

Again, the curves are easy to interprete and need not much comment. High amplification events are mostly, although not in any case, asymmetric, and often the characteristic U-shape appears. For large sources, the light curves are much flatter and more symmetric.

Even for small sources, large portions of the light curves do not show considerable variations, as already mentioned above. For low optical depth, the source is most of the time only weakly magnified, and occasionally large ($\Delta m \gtrsim 2$ –3 for the small sources) variations occur. For high optical depth (e.g., cases e, f, l), the magnification is always high, whereas the variations in Δm are comparatively small.

It is clear that the spatial resolution in our computations is not sufficient to resolve the intensity peaks of the smallest sources. This is, however, not a severe drawback, since in most cases the form of these peaks can be derived analytically. In Appendix B it is shown that the amplification factor of a circular source of radius R at a distance D from the critical line [where D is taken positive for that side of the critical line to which the amplification of a point source diverges, see, e.g., Blandford et al. (1986)] is

$$I(D,R) = I_0 + a_0 R^{-1/2} J(D/R)\,, \tag{20}$$

where the function $J(x)$ is given by (B7, B11) and shown in Fig. B1, and the constants I_0 and a_0 can be obtained from the numerical computations shown in Fig. 2. Note that (20) is only valid if the source crosses an ordinary critical line and not a cusp (cf. Blandford et al., 1986; Schneider and Weiss, 1986). The signature of a crossing of a critical line in the light curves is the

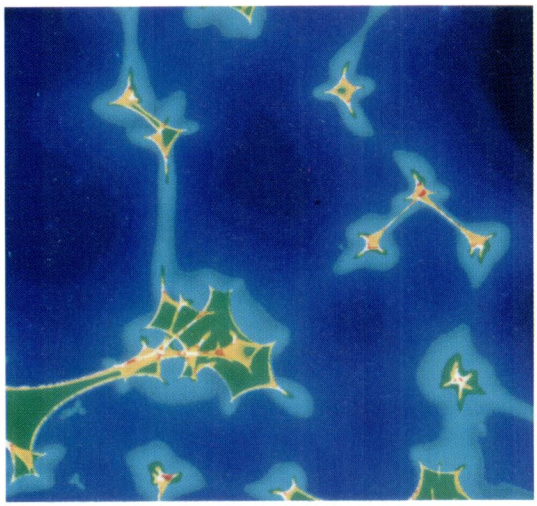

a

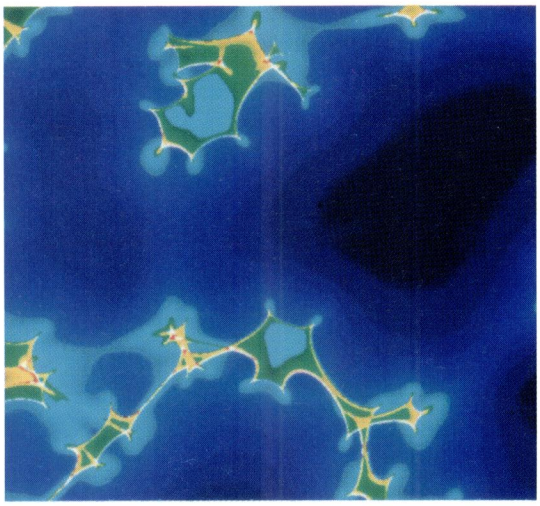

b

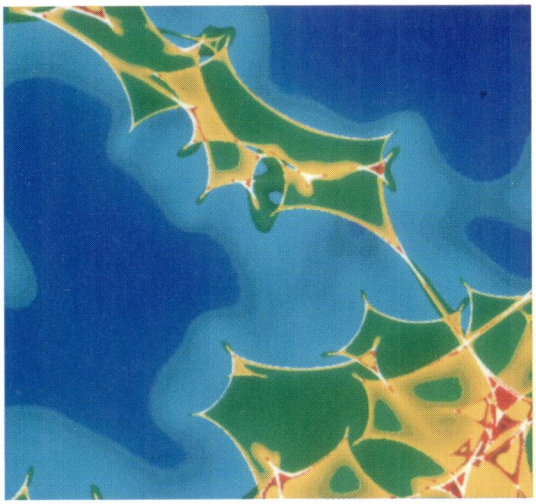

c

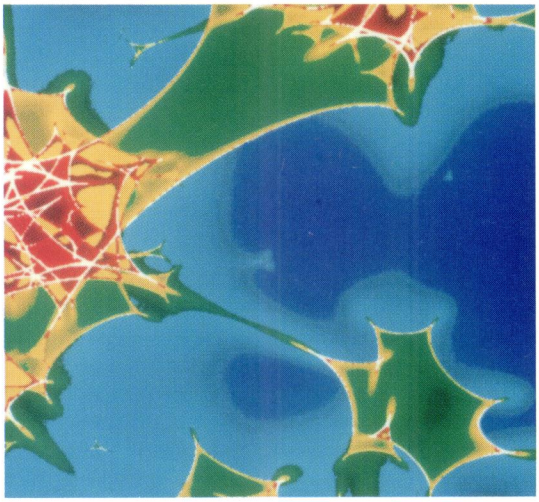

d

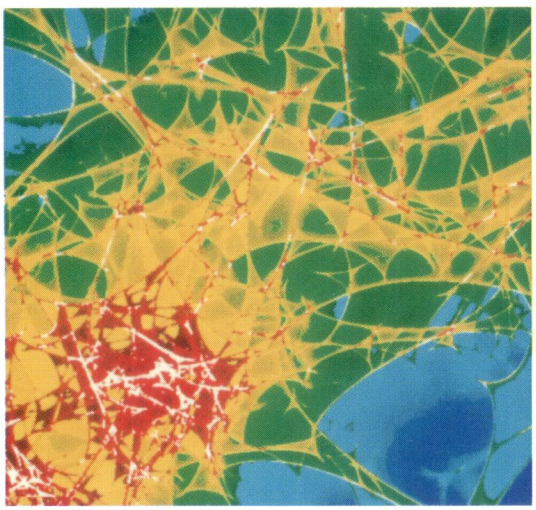

e

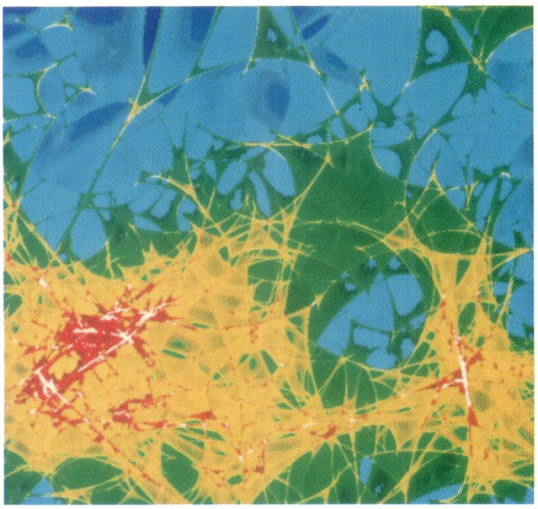

f

Fig. 1a–l. The amplification factor plotted as a function of the relative source position, for the cases a–l described in Table 1. The colour coding is described in the text below Eq. (18) with the values of $\Delta m_{\min}$ and $\Delta m_{\max}$ given in Table 1

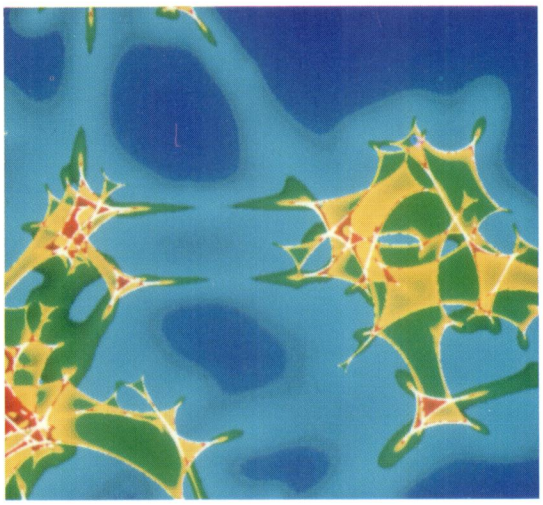

g

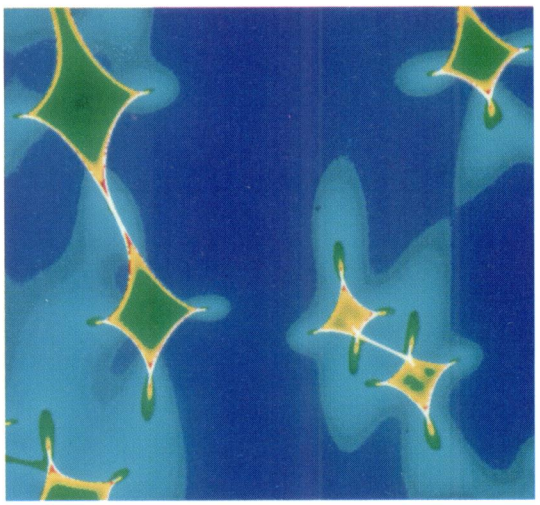

h

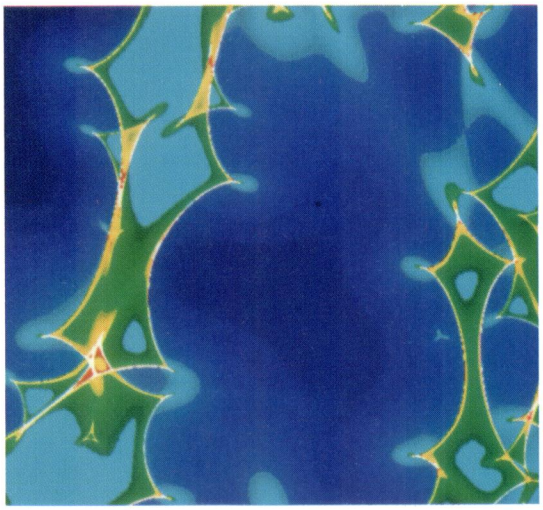

i

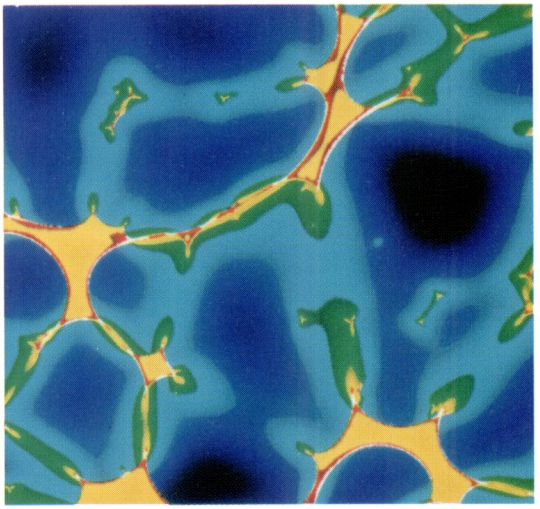

j

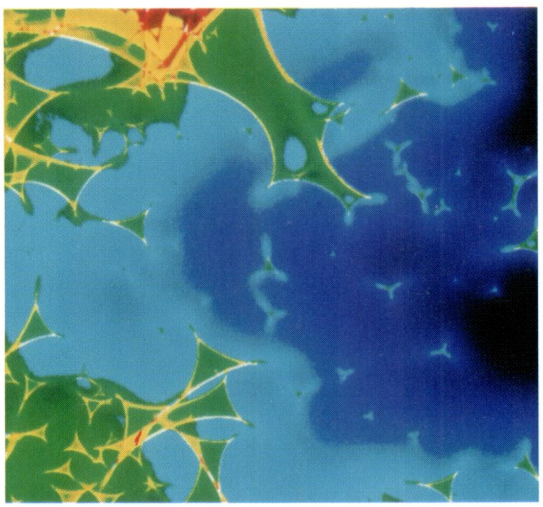

k

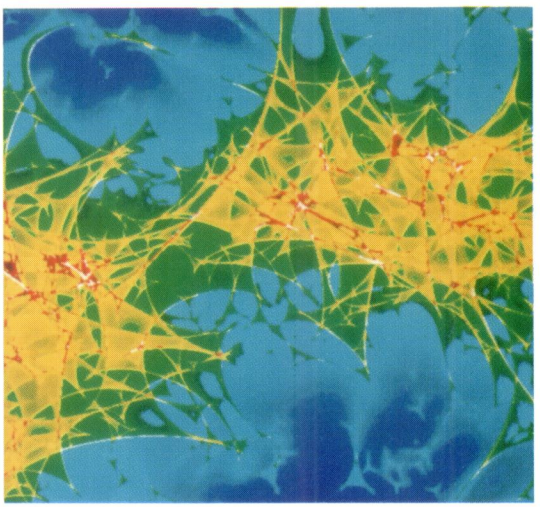

l

Fig. 1a–l (continued)

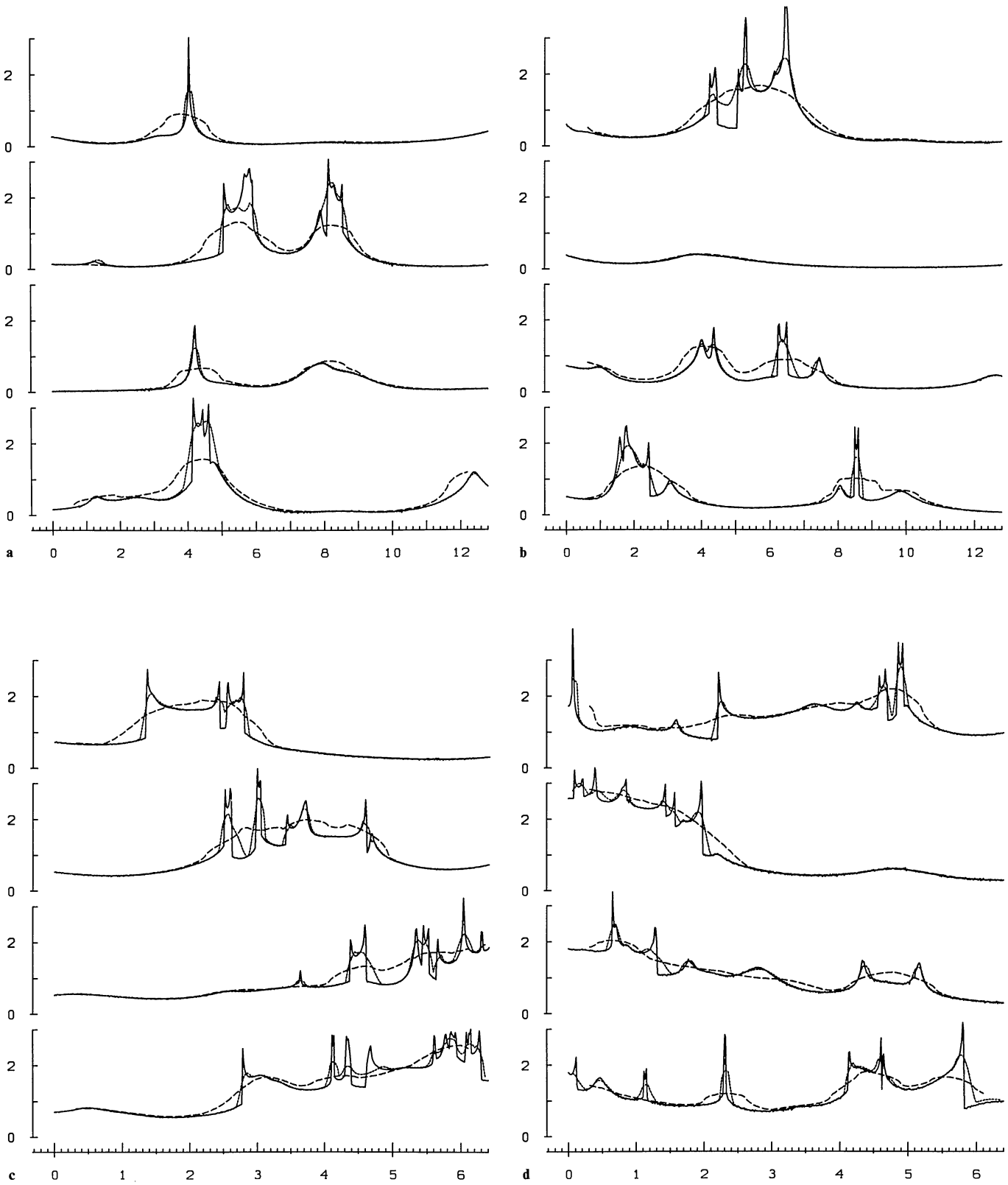

Fig. 2a–l. The magnification Δm (18) as a function of the source position along straight lines through the source plane, shown in Fig. 1, for the cases *a–l* described in Table 1. The solid lines correspond to a source size of *b* (Table 1), whereas the dotted and dashed line correspond to source sizes of 10*b* and 50*b*, respectively. The unit of length along the *x*-axis is χ_0 (3). Considering these curves as light curves, the unit of time along the *x*-axis is τ_0 (19)

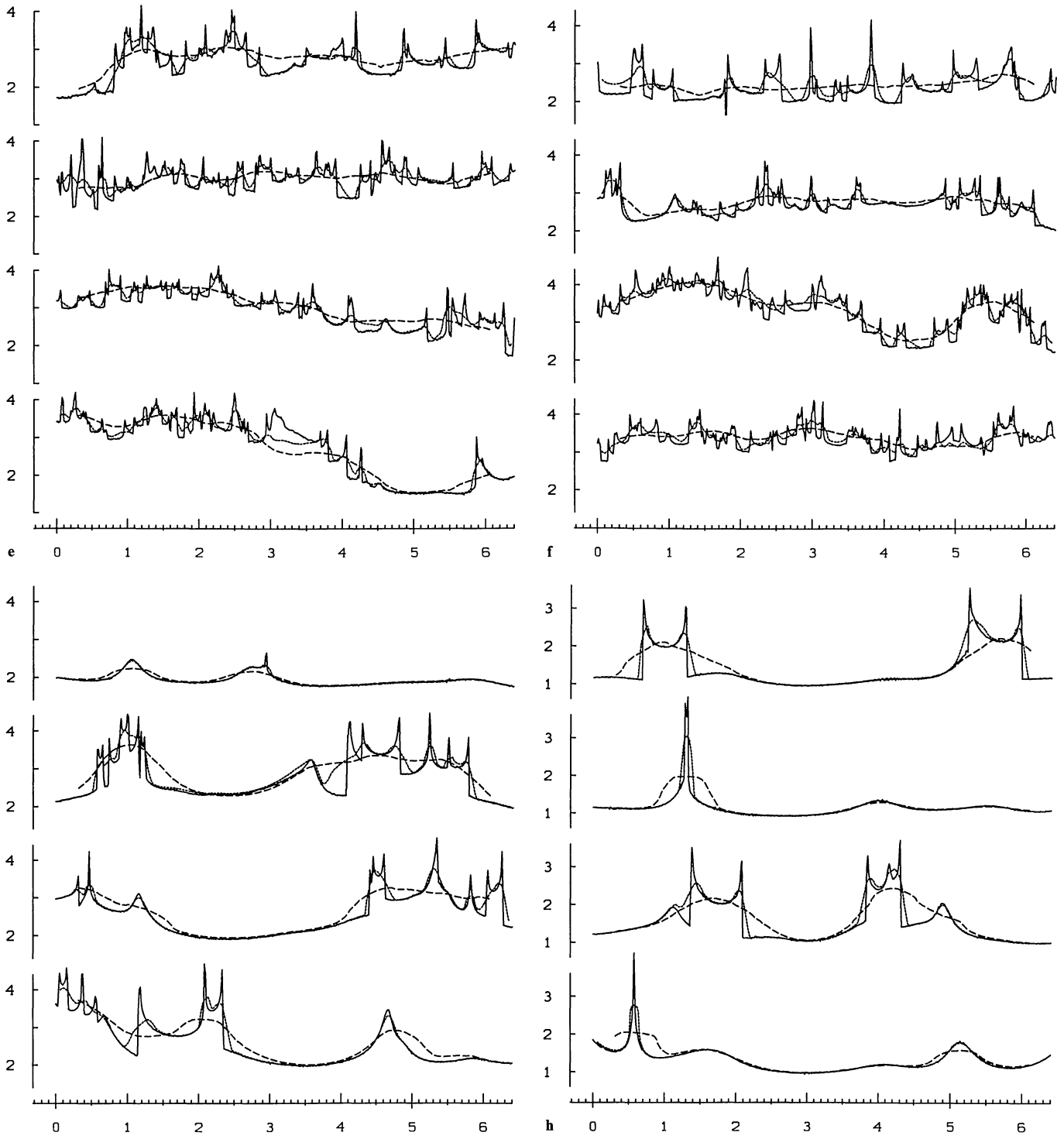

Fig. 2a–l (continued)

typical asymmetric feature near the peaks. The symmetric peaks stem from sources which pass near, but outside, a cusp.

Note that there are basically two time-scales, relevant for light variations. The first one is the typical rise time to a peak in the amplification. From (20) and Fig. B1 one can notice that this corresponds to a displacement of $\Delta x \sim R$ of the source across a critical line; hence, the corresponding time-scale τ_1 is

$$\tau_1 = \tau_0 R, \tag{21}$$

where τ_0 is given by (19) and R is the dimensionless source size, or in terms of the physical source size $\varrho = \chi_0 R$, one has

$$\tau_1 = \varrho / v, \tag{22}$$

where again v is the effective velocity of transverse source motion [KRS, Eq. (B9)].

The second time-scale one is interested in is the time between two peaks. As already mentioned (and clearly visible from Fig. 2)

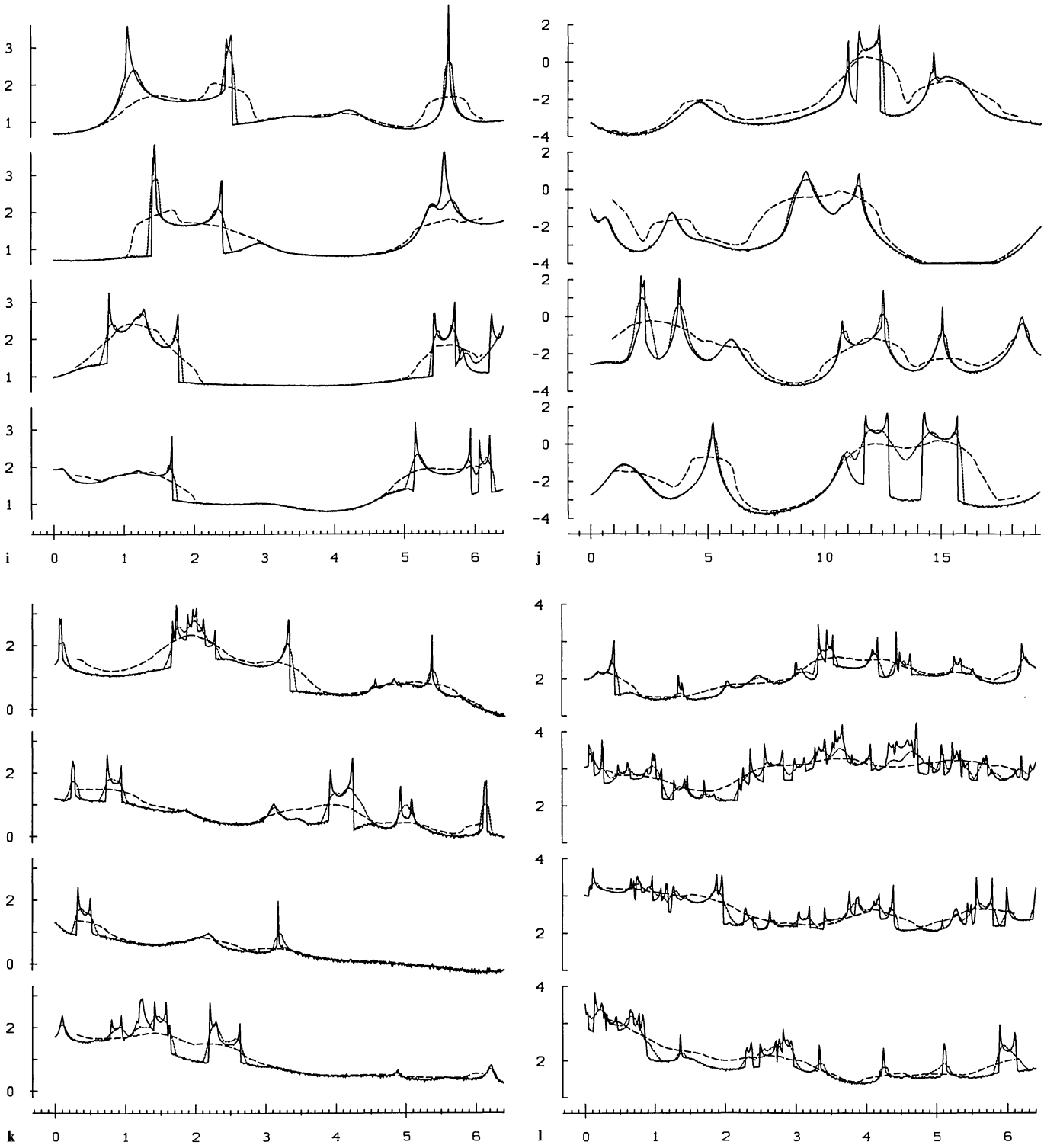

Fig. 2a–l (continued)

this time is much more subject to large statistical fluctuations and is therefore less useful than the rise-time τ_1. From Fig. 2 one can derive a mean time between peaks, τ_2, given as

$$\tau_2 = f \cdot \tau_0 , \tag{23}$$

where the factor f is ~ 4 for $\kappa = 0.2$, ~ 1 for $\kappa = 0.5$ and ~ 0.2 for $\kappa = 0.8$; it thus depends sensitively on the specific lens model.

5.3. Amplification probabilities

From the distribution of the amplification factors shown in Fig. 1, one can determine the probability $P(I)$ that a source is amplified by a factor greater than I. This probability function is shown in Fig. 3a–l for sources of size b, $3b$, $10b$, 30 b, and $100b$ in each case. The maximum amplification obtained in each case depends strongly on the source size.

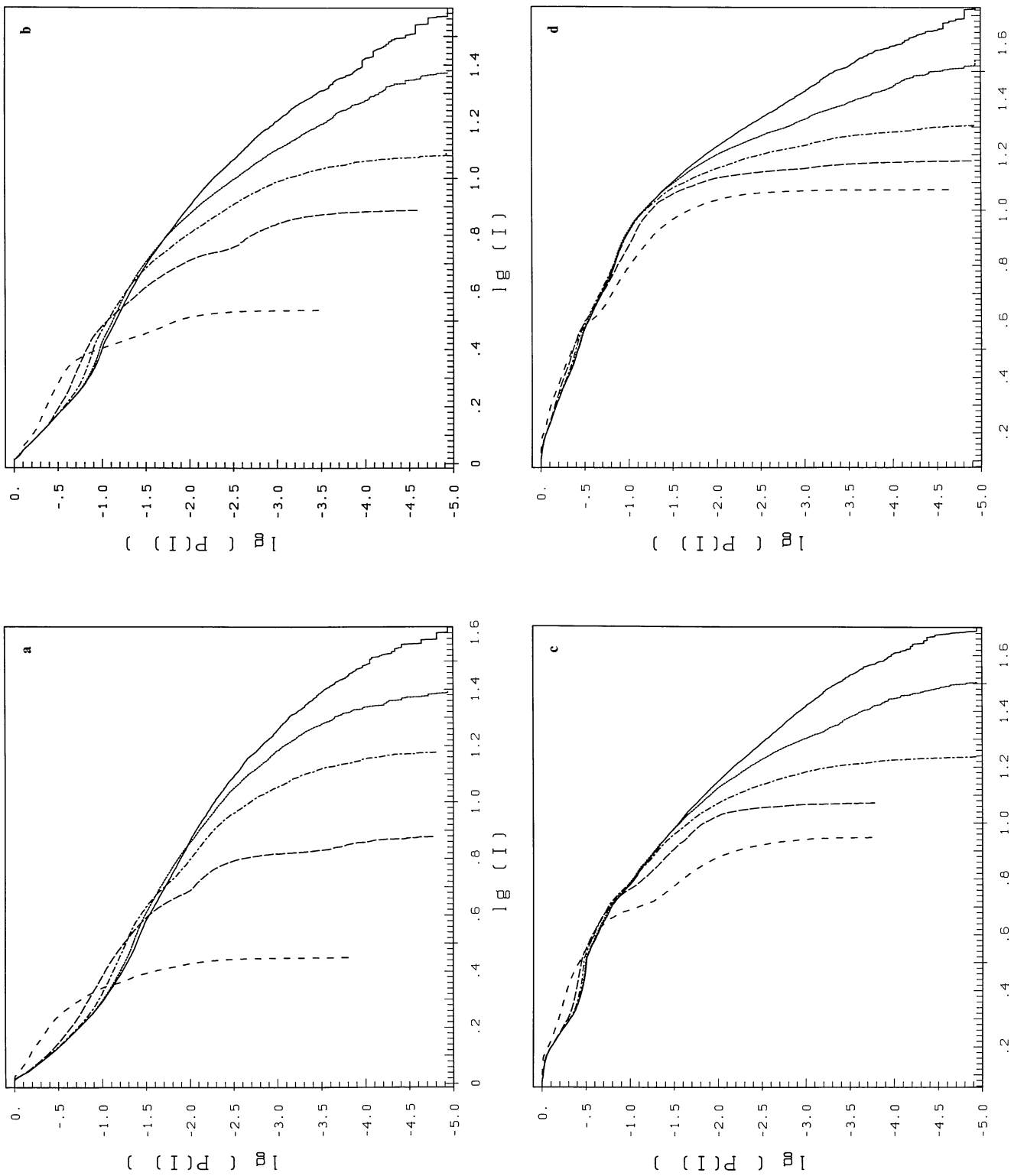

Fig. 3a–l The probability $P(I)$ that a source behind the star field is amplified by a factor larger than I is shown in these log–log plots, which show the cases a–l described in Table 1. In each plot, $P(I)$ is shown for source sizes of b (solid), $3b$ (dotted), $10b$ (dashed-dotted), $30b$ (long dashed), and $100b$ (short dashed line)

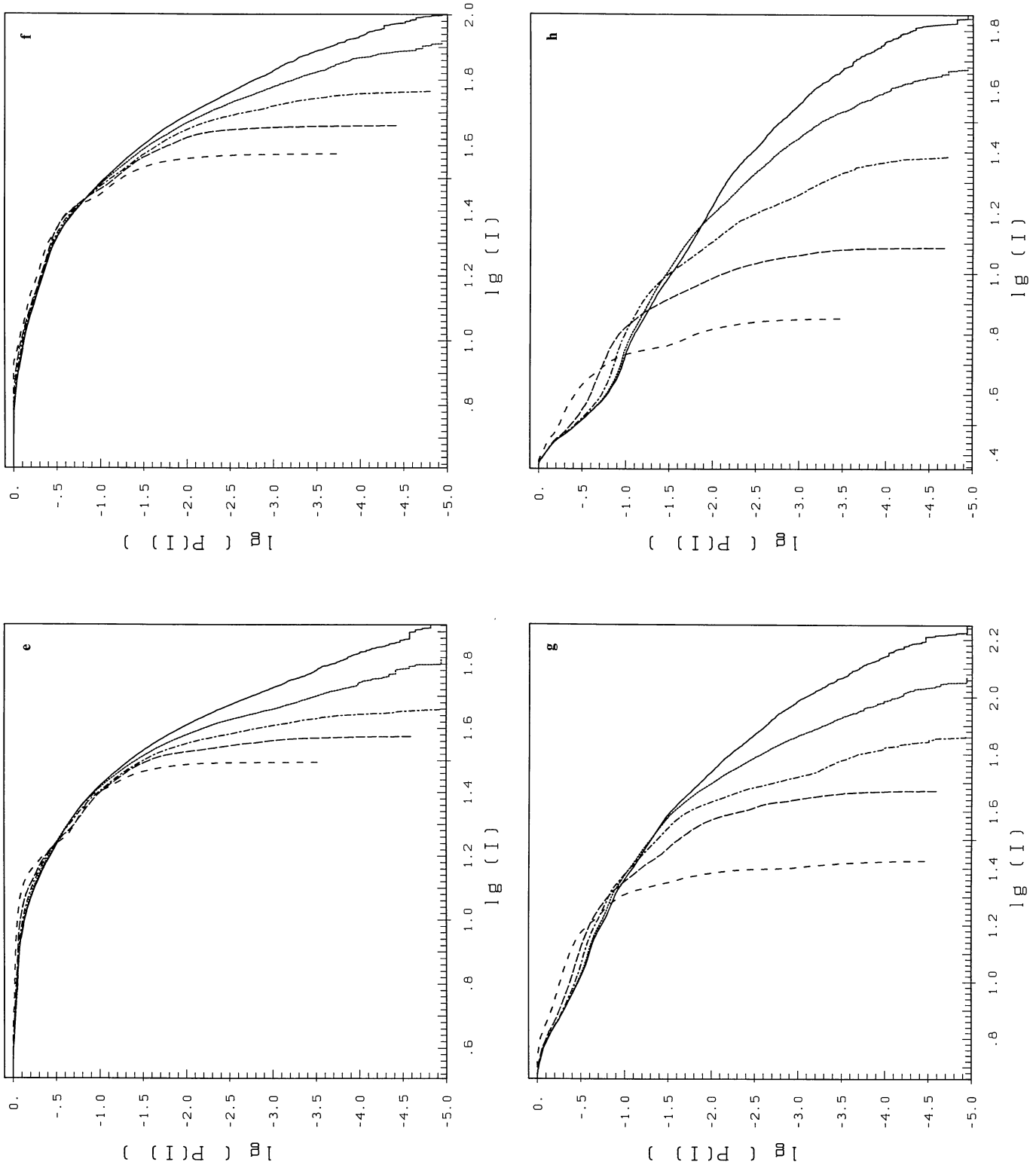

Fig. 3a–l (continued)

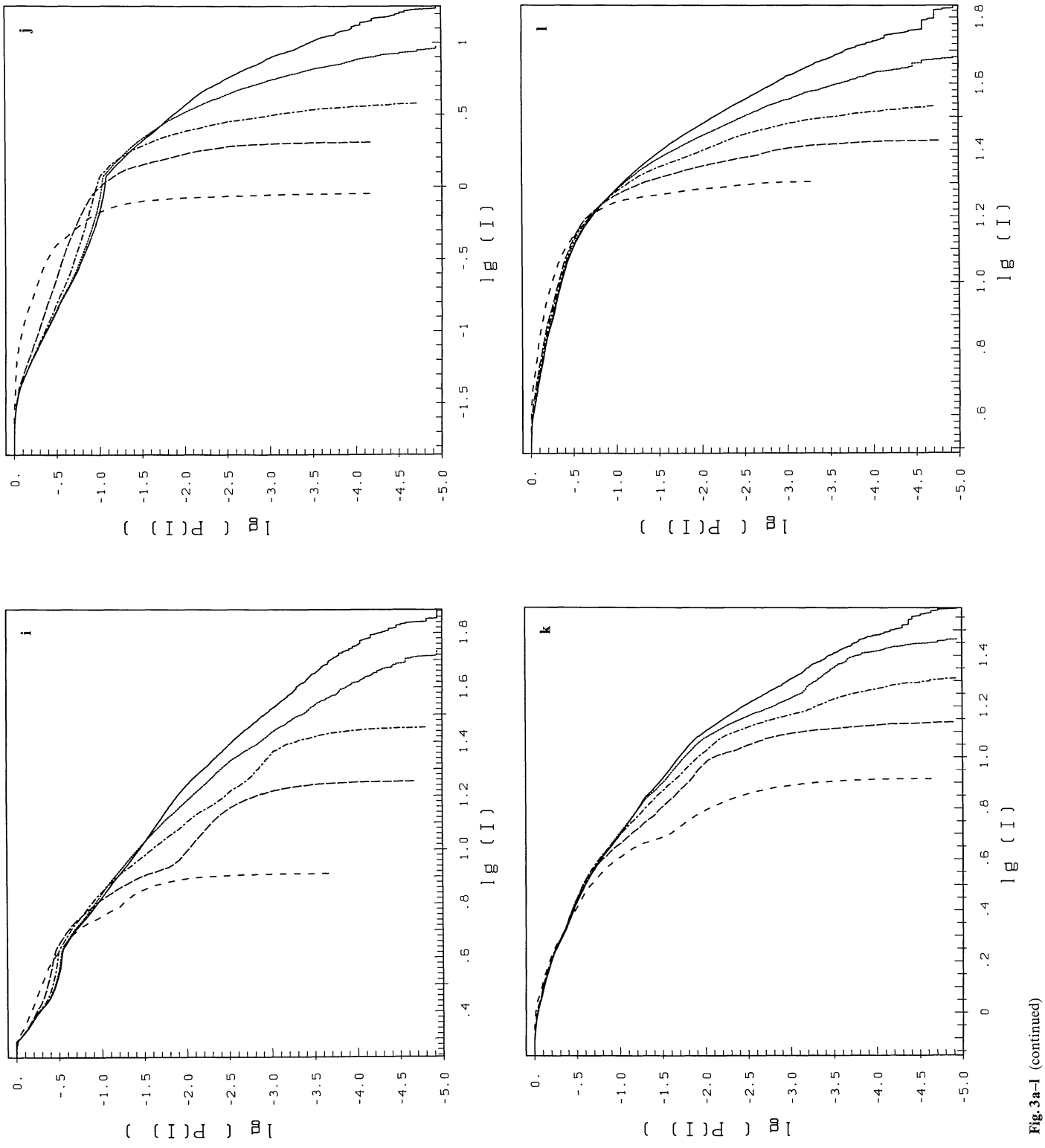

Fig. 3a–l (continued)

In general, the high-I part of the $P(I)$ curve cuts off earlier for larger sources, whereas $P(I)$ is larger for larger sources in the small I regime. It is clearly seen that the $P(I)$ curve shows no I^{-2}-behaviour as usually assumed for small sources (e.g., Canizares, 1981; Vietri and Ostriker, 1983) but shows much more complicated behaviour for all values of I. In some cases (e.g., c, i), the $P(I)$ curve for the smallest source becomes very flat for a specific value of I; from a comparison with the corresponding colour plots one can notice that these values of I are those values at which the amplification factor distribution obtains broad minima (e.g. for case j one has a flat "shoulder" in $P(I)$ at $\lg I \approx 0$; this corresponds to several extended minima in Fig. 1j which have a yellow colour). Due to the above-mentioned clustering of critical structure, the $P(I)$-curves shown can only be considered as probability distribution in a random region of the source plane, and deviate probably from the mean probability distribution.

Due to amplification, the observed density of sources through the star field under consideration is modified. Let $N(S)$ be the number density of sources at a certain redshift z_s with flux greater than S which one observes far away from any galaxy, then the density of sources seen through the star field is

$$N_{\rm obs}(S) = \langle I_s \rangle^{-1} \int dI p(I) N(S/I),$$

where

$$p(I) = -\frac{d}{dI} P(I)$$

is the differential probability distribution, and the factor $\langle I_s \rangle^{-1}$ accounts for the overall area distortion of the lens mapping (see Schneider, 1986b). In particular, for a power law distribution, $N(S) \propto S^{-(\alpha-1)}$, where α is the slope of differential luminosity function at z_s, one obtains

$$Q \equiv \frac{N_{\rm obs}(S)}{N(S)} = \langle I_s \rangle^{-1} \int dI p(I)\, I^{(\alpha-1)}. \qquad (24)$$

We have computed the value of Q from the $P(I)$-curves of Fig. 3 for several values of the source size and the power-law index α. The results are displayed in Table 2. It can be seen that Q is an increasing function of α. The sensitivity of Q on the source size increases with α, but varies among the models. In particular, whereas for models of low optical depth the dependence on the source size is very strong, it is very much weaker for high optical depth. The corresponding relative insensitivity of $P(I)$ on the source size can be seen from Fig. 3, and is due to the fact that for high optical depth, the relative importance of critical lines diminishes compared to extended high-amplification regions.

6. Discussion

We have considered the amplification caused by the gravitational action of random star fields, as a function of the relative position of the background source, extending previous computations of Paczyński (1986) and KRS. Since especially the latter paper presents a very clear discussion on the applications of this microlensing on known cases of gravitational lensing, we can limit the discussion here to a few points.

In contrast to the claim of Paczyński that multiple-star effects become important for optical depth larger than 0.5, we find here that even for much lower optical depth ($\lesssim 0.1$) the effects of multiple stars can not be neglected. This is due to the tendency of critical lines to cluster.

The results for high optical depth (e.g., cases e, f, and l) show that one can obtain very high amplification factors of a source, but without large intensity changes similar to outburst, but more with a flicker of the source, i.e. brightness variations of ~ 0.5 mag. As an example, consider the B-image of QSO 0957+561 (Walsh et al., 1979) for which the optical depth is expected to be very high. In this case, $\chi_0 \approx 5\ 10^{16}$ cm for solar mass lenses, hence our smallest source size $b = 0.0125$ for the cases of high optical depth corresponds to $\sim 6\ 10^{14}$ cm. If the continuum source is not smaller than this, large changes of brightness cannot be expected. In fact, if the source is a factor ~ 10 larger than the value given above, the expected light curves should be rather smooth.

The broad absorption-line QSO IE 0104+315 (Stocke et al., 1984) has $z_s = 2.03$ and is seen through a giant elliptical galaxy at $z_d = 0.11$, only 10 arcsecs away from its center. Using the parameters of Stocke et al., we find that this case probably corresponds to our $\kappa_* = 0.2$, $\kappa_c = 0$ computations (cases a and b); hence, the light curves in Fig. 2a and b should apply in that case. Supposing that the relevant transverse motion is given by the transverse velocity v_d of the local star field, relative to the line-of-sight to the quasar, one obtains for solar mass objects

$$\tau_0 \approx (v_d/1000\ \text{km/s})^{-1}\ 7.5\ \text{yr},$$

$$\tau_1 \approx (\varrho/10^{15}\ \text{cm})\,(v_d/1000\ \text{km/s})^{-1}\ \text{months},$$

and

$$\chi_0 \approx 10^{17}\ \text{cm};$$

hence, for a source of size $\sim 10^{15}$ cm the solid curves in Fig. 2a and b are applicable. The time-scale τ_0 implies that one should observe intensity peaks of that source, on the average, every ~ 30 yr; however, as discussed earlier, this number is subject to large statistical spread.

Beside the analysis of known cases of gravitational macrolensing, where our results can yield a large number of astrophysical informations (e.g., nature of galactic halos, source size and structure; see the discussion in KRS), the main application we have in mind is of a statistical nature. As was shown by Schneider (1986d), even a small density of compact objects in the universe has a major influence on the observed luminosity function of AGNs, provided the intrinsic luminosity function is sufficiently steep (as, e.g., indicated by the results of Veron, 1983) and the source size ϱ satisfies $\varrho \lesssim 10^{17}\,(M/M_\odot)^{1/2}$ cm, as indicated by variability time-scales. If most of the amplification occurs by compact objects in galaxies, the lensed AGNs should show light variations similar to that in Fig. 2. However, the situation may be more complex, if the source, in one spectral band, is composed of several components. There are some good arguments in favour of this possibility. Malkan and Moore (1986) have found that the optical continuum of some quasars (including the prototype, 3C273, see Impey and Malkan, 1986) is composed of at least three components: a "blazar" component, characterized by its variability, high polarization and a steep power-law spectrum, a "normal" quasar component, which has a flatter spectrum, and the quasi-thermal UV-bump. VLBI-observations usually show the multi-component nature of compact radio sources. The rapid changes in the degree and position angle of polarization in some blazars (see, e.g., Angle and Stockman, 1980) is sometimes explained by independent luminosity variations of many highly polarized components. If the different components are spatially separated, the light curves of lensed objects may show quite different behaviour from those shown in Fig. 2.

The above-mentioned findings of Malkan and Moore must also be seen in view of a recent suggestion by Ostriker and Vietri (1985), that (some) BL Lac objects can be explained as gravitationally (micro-)lensed and highly amplified quasars. In the light of our result and those obtained by Schneider (1986d), we view this hypothesis to be quite likely. In particular, there are some objects which during their high luminosity stage appear as a BL Lac object, whereas they turn into a "normal" quasar at lower luminosity (see, e.g., Arp et al., 1979). More general, the selective amplification provided by micro-lensing may well change the classification of an AGN. Since the probability to observe sources being micro-lensed depends on the intrinsic luminosity function of the parent population, this possible mixing of AGN classes by lensing furthermore complicates the estimate of the probability (see Schneider, 1986d).

We finally ask whether light variations similar to those shown in Fig. 2 have actually been observed. Consider first the time-scales involved. The time-scale for rapid luminosity rise (and decline) τ_1 (22) is a factor c/v larger than the light crossing time in the source. Hence, if the relevant source component moves relativistically, these two time-scales agree. The only direct evidence of relativistic motion in AGN comes from VLBI observations of superluminal sources. Note that the fraction of superluminal sources among compact radio sources is high (Porcas, 1985). Of course, it is unknown how many AGN have relativistically moving source components, but there is no reason to assume this fraction to be small. Thus, it is no problem to account for variability time-scales by lensing.

Lens-induced variability should cause light curves which are symmetric on the average (where the average has to be taken over several "outbursts"). We don't see any evidence for pronounced asymmetry in the optical light curves presented by the group at Rosemary Hill (see Pica and Smith, 1983, and references therein). The same is true for the radio light of BL Lac (Johnston et al., 1984), a source for which relativistic motion is established (Mutel et al., 1981). Another prediction of our model, which can be seen from Fig. 2, is that sources which are lensed by star fields of moderate ($\tau \sim 0.5$) optical depth should show phases of high "activity", with rather quiet phases in between. This has been observed for several sources; e.g., BL Lac was very active between 1969 and 1973, but quiet from 1974 to 1980, where it became active again. The quasar 1156+295, one of the most extremely variable objects, was very inactive from 1950 to 1977, but active earlier in the century and after 1977.

We are quite convinced that micro-lensing can account for the variability of at least some AGN, and hope that this paper will induce more discussions on this topic; especially, since it seems to be a viable possibility to get rid of apparent super-Eddington luminosity sources.

Appendix A: Scaling

In this Appendix we derive the scaling Eqs. (7a)–(7d) by using the method of Paczyński (1986). We start from the lens Eq. (6), written in the form

$$\boldsymbol{x} = \begin{pmatrix} 1-\kappa_c-\gamma & 0 \\ 0 & 1-\kappa_c+\gamma \end{pmatrix} \boldsymbol{r} - \sum_{i=1}^{N_*} \frac{\boldsymbol{r}-\boldsymbol{r}_i}{|\boldsymbol{r}-\boldsymbol{r}_i|^2}. \tag{A1}$$

Defining, for $\kappa_c \neq 1$,

$$\boldsymbol{X} = |1-\kappa_c|^{-1/2}\,\boldsymbol{x}, \tag{A2a}$$

$$\boldsymbol{R} = |1-\kappa_c|^{1/2}\,\boldsymbol{r}, \tag{A2b}$$

$$\boldsymbol{R}_i = |1-\kappa_c|^{1/2}\,\boldsymbol{r}_i, \tag{A2c}$$

this can be rewritten as

$$\boldsymbol{X} = \begin{pmatrix} 1-\Gamma & 0 \\ 0 & 1+\Gamma \end{pmatrix} \boldsymbol{R} - \sum_{i=1}^{N_*} \frac{\boldsymbol{R}-\boldsymbol{R}_i}{|\boldsymbol{R}-\boldsymbol{R}_i|^2}, \tag{A3}$$

where

$$\Gamma = \frac{\gamma}{|1-\kappa_c|}. \tag{A4}$$

The Eqs. (A2a)–(A2c) correspond to a change of the length scales in the source and lens planes. Equation (A3) contains no κ_c at all and is, therefore, valid for all $\kappa_c \neq 1$. Hence, the transformation leading from (A1) to (A3) can be used to find the scaling relations between models of different κ_c.

Consider first a model with vanishing interstellar surface mass density, $\kappa_c = \kappa_c^* = 0$, in which case (A1) and (A3) are formally identical. The length scale in the lens plane ξ_0^* is related to ξ_0 for the κ_c model described by (A1) through

$$\xi_0^* = \frac{\xi_0}{|1-\kappa_c|^{1/2}}, \tag{A5}$$

which is derived by considering a physical length $\xi = \xi_0 r = \xi_0 |1-\kappa_c|^{-1/2} R$. Similarly, the length scales in the source plane are related through

$$\chi_0^* = \chi_0 |1-\kappa_c|^{1/2}. \tag{A6}$$

Suppose the N_* stars in (A1) are distributed over an ellipse of semi-axis B and D. Then, the density of stars κ_* is given by

$$\kappa_* = \frac{N_*}{BD};$$

due to the scaling (A2c), in the $\kappa_c^* = 0$ model the N_* stars are spread over an ellipse of semi-axis $B^* = |1-\kappa_c|^{1/2} B$, $D^* = |1-\kappa_c|^{1/2} D$, and therefore,

$$\kappa_*^* = \frac{N_*}{B^* D^*} = \frac{\kappa_*}{|1-\kappa_c|}. \tag{A7}$$

The total amplification factor I of a point source is the sum of the amplification of all images, i.e.

$$I = \sum_k \left| \det \left(\frac{\partial \boldsymbol{x}}{\partial \boldsymbol{r}} \right)_k \right|^{-1},$$

where the sum is taken over all images of the source at $\boldsymbol{x}$. Since (A2) implies

$$\det \left(\frac{\partial \boldsymbol{x}}{\partial \boldsymbol{r}} \right) = |1-\kappa_c|^2 \det \left(\frac{\partial \boldsymbol{X}}{\partial \boldsymbol{R}} \right),$$

one obtains

$$I^* = |1-\kappa_c|^2 I. \tag{A8}$$

By use of (A6), one finds that the amplification factors of extended sources are related through (A8), if the dimensionless source sizes satisfy

$$b^* = |1-\kappa_c|^{-1/2} b. \tag{A9}$$

Since the starred quantities are independent of κ_c, the scaling Eqs. (7a)–(7d) can now be read off from (A4), (A7), (A9), and (A8), respectively.

Appendix B: Amplification of extended sources near a critical line

It is well-known that the number of images of a source changes by two if and only if the source position changes across a critical line (Bourassa and Kantowski, 1975; Chang and Refsdal, 1979, 1984; Schneider and Weiss, 1986; Blandford et al., 1986). In these papers, it was shown that the amplification factor of a point source near a critical line is

$$I_p(x) = I_0 + \theta(x)\, a_0\, x^{-1/2}, \tag{B1}$$

where x is the perpendicular distance to the critical line and two images are created (destroyed) if the source crosses the critical line from negative to positive (positive to negative) x. I_0 is the amplification of all other images of the source, usually slowly varying with x, and therefore taken to be constant over the region under consideration, compared to that of the two "critical" images, the amplification of which is given by the second term in (B1). Here, $\theta(x)$ is the Heaviside step function, and a_0 is a constant, depending on the details of the lens mapping near the critical line.

The amplification I of an extended source with surface brightness distribution $\Upsilon(\boldsymbol{x})$ is obtained as a weighted average of the point source amplification over the source, i.e.

$$I = [\int d^2x\ \Upsilon(\boldsymbol{x})\ I_p(\boldsymbol{x})]/[\int d^2x\ \Upsilon(\boldsymbol{x})], \tag{B2}$$

where the integrals are taken over the support of Υ.

We choose a coordinate frame in which the critical line is locally described by $x = 0$. Consider a circular source of radius R the center of which has the coordinates $(D, 0)$. We will treat two different cases here:

1. *Source of uniform brightness*

In this case, one has

$$\Upsilon(x, y) = \theta\,[R^2 - (x - D)^2 - y^2]. \tag{B3}$$

Inserting this into (B2), integrating over y and using (B1) yields

$$I(D, R) = I_0 + \frac{2a_0}{R^2\pi} \int_{\max(0, D-R)}^{\max(0, D+R)} dx\,[R^2 - (x - D)^2]^{1/2}\, x^{-1/2}. \tag{B4}$$

Substituting $z = (x - D)/R$ and defining $d = D/R$, one finds

$$I(D, R) = I_0 + a_0 R^{-1/2}\, J(D/R), \tag{B5}$$

where

$$J(d) = (2/\pi) \int_{\max(-d, -1)}^{\max(-d, +1)} dz\,(1 - z^2)^{1/2}\,(z + d)^{-1/2}. \tag{B6}$$

Using Eqs. (3.141.34) and (3.141.28) of Gradshteyn and Ryzhik (1980, hereafter GR), on obtains

$$J(d) \begin{cases} 0 & \text{for } d < -1 \\ \dfrac{4 \cdot 2^{1/2}}{3\pi} \left\{(1 - d)\, K\left[\left(\dfrac{1 + d}{2}\right)^{1/2}\right] + 2d\, E\left[\left(\dfrac{1 + d}{2}\right)^{1/2}\right]\right\}, & \text{for } -1 < d < 1 \\ \dfrac{8}{3\pi}(1 + d)^{1/2} \left\{dE\left[\left(\dfrac{2}{1 + d}\right)^{1/2}\right] - (d - 1)\, K\left[\left(\dfrac{2}{1 + d}\right)^{1/2}\right]\right\}, & \text{for } 1 < d \end{cases} \tag{B7}$$

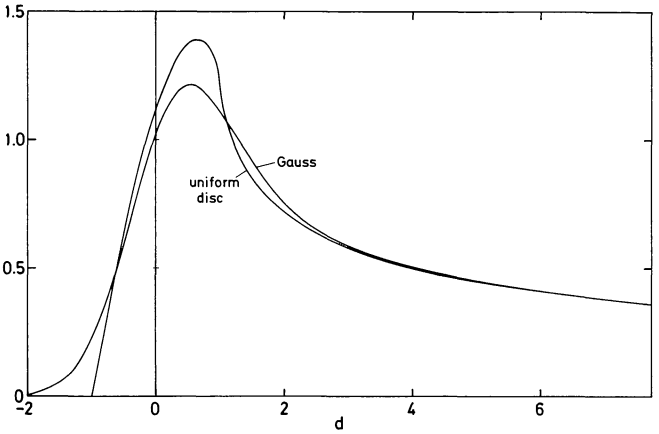

Fig. B1. The function $J(d)$ for sources of uniform brightness (B7) and Gaussian brightness distribution (B11)

where $K(x)$ and $E(x)$ are the complete elliptical integrals of the first and second kind, respectively (see GR, 8.11). The function $J(d)$, which is plotted in Fig. B1, determines the shape of the light curve of a source which crosses the critical line. The amplitude of the light curve is solely determined by a_0 and R. The non-smoothness of $J(d)$ at $d = -1$ is due to the discontinuous surface brightness distribution. Note the asymmetry of $J(d)$, also seen in Fig. 2 of the main text: it rises steeply from $d = -1$ to its maximum at $d = 2/3$; then it declines even steeper, reaching a turning point at $d \approx 1$ and then it approaches the asymptotic $d^{-1/2}$ behaviour.

2. *Source with Gaussian brightness distribution*

Here one has

$$\Upsilon(x, y) = \exp\left[-\frac{(x - D)^2 + y^2}{R^2}\right], \tag{B8}$$

which after inserting into (B2) leads to the same Eq. (B5) as in the case of a uniform brightness disk, but where now the function $J(d)$ is given by

$$J(d) = \pi^{-1/2}\, e^{-d^2} \int_0^\infty dx\, e^{-x^2 + 2xd}\, x^{-1/2}. \tag{B9}$$

This can be integrated, using Eq. (3.462.1) of GR to yield

$$J(d) = 2^{-1/4}\, e^{-d^2/2}\, D_{-1/2}(-2^{1/2} d), \tag{B10}$$

where $D_\nu(x)$ is the parabolic cylinder function of degree ν. Using the notation of Abramowitz and Stegun (1965, hereafter AS), one has $D_\nu(x) = U(-\nu - \frac{1}{2}, x)$ [AS, Eq. (19.3.1)]. An alternative expression for $J(d)$ is obtained by making use of Eq. (19.15.9) of AS:

$$J(d) = 2^{-3/4}\, \pi^{-1/2}\, e^{-d^2/2}\, d^{1/2}\, K_{1/4}(-2^{1/2} d), \tag{B11}$$

where $K_\nu(x)$ is the modified Bessel function of order ν (AS, Chap. 9).

The function $J(d)$ (B10) is also plotted in Fig. B1, showing that it is not as steep as the corresponding function (B7) for a uniform disk. The maximum value at $d \approx 0.541$ is less and the curve is broader than (B7). However, for $d \gtrsim 3$ both curves basically agree, showing $d^{-1/2}$ behaviour.

Since the two surface brightness distributions we considered here are both extreme, in the sense that the uniform disk has an extremely sharp edge, whereas the Gauss source is extremely smooth, we expect that other models for the brightness distribution lead to light curves similar to those shown in Fig. B1.

References

Abramowitz, M., Stegun, I.A.: 1965, Handbook of Mathematical Functions, Dover, New York (AS)

Angle, J.R.P., Stockman, H.S.: 1980, *Ann. Rev. Astron. Astrophys.* **18**, 321

Arp, H., Sargent, W.L.W., Willis, A.G., Oosterbaan, C.E.: 1979, *Astrophys. J.* **230**, 68

Blandford, R.D., Narayan, R., Nityananda, R.: 1985 (preprint)

Bourassa, R.R., Kantowski, R.: 1975, *Astrophys. J.* **195**, 13

Canizares, C.R.: 1981, *Nature* **291**, 620

Canizares, C.R.: 1982, *Astrophys. J.* **263**, 508

Chang, K., Refsdal, S.: 1979, *Nature* **282**, 561

Chang, K., Refsdal, S.: 1984, *Astron. Astrophys.* **132**, 168

Gott, J.R.: 1981, *Astrophys. J.* **243**, 140

Gradshteyn, I.S., Ryzhik, I.M.: 1980, Table of Integrals, Series and Products, Academic Press, New York (GR)

Impey, C.R., Malkan, M.A.: 1986 (in preparation)

Johnston, K.J., et al.: 1984, *Astrophys. J.* **277**, L31

Katz, N., Balbus, S., Paczyński, B.: 1986, *Astrophys. J.* **306**, 2

Kayser, R., Refsdal, S., Stabell, R.: 1986, *Astron. Astrophys.* (accepted) (KRS)

Malkan, M.A., Moore, R.L.: 1986, *Astrophys. J.* **300**, 216

Mutel, R.L., Aller, H.D., Phillips, R.B.: 1981, *Nature* **294**, 236

Ostriker, J.P., Vietri, M.: 1985, *Nature* **318**, 446

Paczyński, B.: 1986, *Astrophys. J.* **301**, 503

Pica, A.J., Smith, A.G.: 1983, *Astrophys. J.* **272**, 11

Porcas, R.W.: 1985, in: *Active Galactic Nuclei*, ed. by J.E. Dyson, Manchester

Refsdal, S.: 1964, *Monthly Notices Roy. Astron. Soc.* **128**, 295

Schneider, P.: 1985, *Astron. Astrophys.* **143**, 413

Schneider, P.: 1986a, *Astrophys. J.* **300**, L31

Schneider, P.: 1986b, *Astron. Astrophys.* (submitted)

Schneider, P.: 1986c, *Astron. Astrophys.* (submitted)

Schneider, P.: 1986d, *Astron. Astrophys.* (submitted)

Schneider, P., Weiss, A.: 1986, *Astron. Astrophys.* **164**, 237

Stocke, J.T., Liebert, J., Schild, R., Gioia, I.M., Maccarcaro, T.: 1984, *Astrophys. J.* **277**, 43

Veron, P.: 1983, in *Quasars and Gravitational Lenses*, ed. J.P. Swings, Liège

Vietri, M.: 1985, *Astrophys. J.* **293**, 343

Vietri, M., Ostriker, J.P.: 1983, *Astrophys. J.* **267**, 488

Walsh, D., Carswell, R.F., Weymann, R.J.: 1979, *Nature* **279**, 381

Young, P.: 1981, *Astrophys. J.* **244**, 756